Waveform Parameter Design and Comparisons for Millimeter-Wave Massive MIMO Systems with RF Distortions

A. Khansefid[1], H. Minn[1], Q. Zhan[1], N. Al-Dhahir[1], H. Huang[2], and X. Du[2]
[1] The University of Texas at Dallas, Richardson, TX, USA
[2] Huawei Technologies Co., Ltd., Shenzhen, China

***Abstract*—Millimeter-wave (mmWave) massive MIMO systems enable very high data rate applications for 5G systems, but they also face the challenging issues of strong RF distortions and constraints on computational complexity due to very high sampling rate. The choice of waveform and its parameter settings plays an important role in addressing these challenges. This paper studies orthogonal frequency division multiplexing (OFDM) and single carrier frequency domain equalization (SC-FDE) for mmWave massive MIMO systems under strong phase noises, frequency offsets, inphase and quadrature imbalances, power amplifier nonlinearity, and sampling frequency and time offsets. The effects of waveform parameter setting are investigated. The bit error rate, peak-to-average power ratio and power spectral density are evaluated. Our results indicate that the subcarrier spacing is a crucial parameter that influences the performance, and OFDM offers a slight bit error rate (BER) performance advantage over SC-FDE for both the downlink and uplink of mmWave systems under strong RF distortions.**

***Index Terms*—millimeter-wave, RF distortions, sub-carrier spacing, OFDM, single carrier**

I. Introduction

Millimeter-wave (mmWave) communications is one of the promising 5G technology candidates for very high data rate applications [1]. However, it has its own challenges including strong RF distortions (RFD) and high computational complexity due to the very high sampling rate. In addressing these challenges, the choice of the transmission waveform and its parameter settings play an important role. Current 4G systems use two waveforms, namely, OFDM or orthogonal frequency division multiple access (OFDMA) and SC-FDE or single carrier frequency division multiple access (SC-FDMA). There also exist other waveform proposals [2]–[6] for 5G systems which yield better spectral side-lobes at the cost of higher complexity. In view of the high complexity burden in the mmWave regime and to ensure backward compatibility with the current 4G systems, OFDM and SC-FDE are attractive waveform choices. Thus, in this paper we investigate OFDM and SC-FDE as candidate waveforms and compare them for mmWave massive MIMO systems under strong RF distortions.

There exist several works comparing performances of OFDM/OFDMA and SC-FDE/SC-FDMA. Representative works include performance comparison in terms of peak-to-average power ratio (PAPR) [7], PAPR, multi-user diversity gain and scheduling [8], capacity and data rate [9]–[11], scheduling aspects [12], and study of localized SC-FDMA and interleaved SC-FDMA versus OFDMA for a satellite link [13]. However, the above works do not consider mmWave systems with RF distortions. A recent work in [14] characterized desirable waveform features for mmWave systems and presented performance comparison of single and multiple carrier waveforms in terms of PAPR and spectral efficiency based on Shannon capacity. However, several RF distortions were not considered in its performance evaluation.

There also exist several works addressing RF distortions in the literature. [15] considered MIMO-OFDM with phase noise (PN) and carrier frequency offset (CFO) at both transmitter (TX) and receiver (RX) sides. [16] proposed a blind approach for tracking the PN in single-carrier systems with null prefix in 72 GHz. The study in [17] showed that for high coding rate, SC-FDMA systems using rotated constellation could potentially outperform OFDM systems in the presence of PN and channel estimation errors. [18] considered joint in-phase and quadrature imbalance (IQI) and power amplifier (PA) non-linearity pre-distortion design for mmWave transmitters. However, the above studies addressed only a subset of the RF distortions experienced in mmWave systems. Very recently, [19] evaluated effects of PN, IQI, PA, and ADC resolution *individually* on BER performance of mmWave systems with OFDM and SC-FDE. However, it did not investigate combined effects of those hardware impairments.

With regard to the waveform parameter settings, [20] analyzed the PN effects on OFDM sub-carrier spacing. [21] investigated user-specific sub-carrier spacing for OFDM and universal filtered (UF)-OFDM depending on the mobile speed. [22] presented waveform parameter settings for 5G small-cell scenarios. However, these works have not considered effects of several RF distortions.

In this paper, we consider a mmWave massive MIMO system with strong PN, fractional CFO, and IQI at both TX and RX sides as well as power amplifier nonlinearity. We study performance comparison between OFDM and SC-FDE under such systems as well as their waveform parameter settings. Such study is important for successful development and commercialization of practical mmWave systems, but it has not been investigated in the literature since all the existing works addressed only some subsets of these issues.

Notation: Vectors (matrices) are denoted by bold face small (big) letters. The superscripts * and T stand for conjugate and transpose. $\Re\{\cdot\}$ and $\Im\{\cdot\}$ denote real part and imaginary part.

II. Signal Model with RF Distortions

We present the signal model based on OFDM since SC-FDE is simply DFT-precoded OFDM. The transmitter has U_T

978-1-5090-2482-7/16/$31.00 ©2016 IEEE

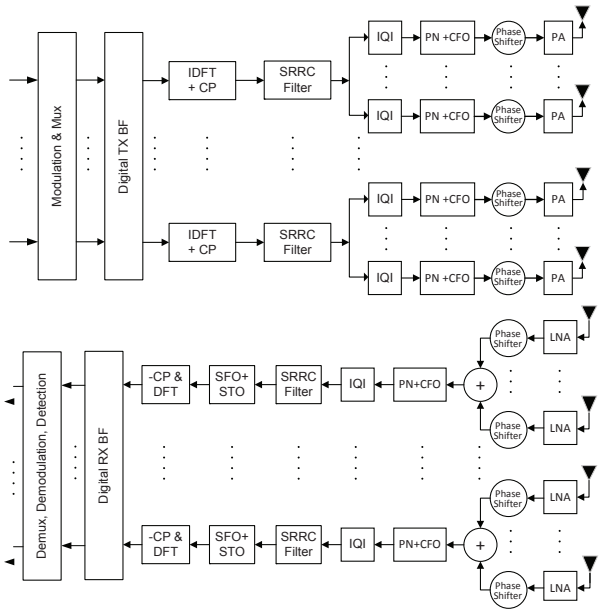

Fig. 1. MIMO-OFDM signal model block diagram with RF impairments. (SRRC = square-root raised cosine filter, PA = power amplifier, LNA = low-noise amplifier, SFO = sampling frequency offset, STO = sampling time offset, BF = beam-forming, CP = cyclic prefix)

digital-to-analog conversion (DAC) branches and each branch is connected to V_T antenna elements. The receiver has U_R analog-to-digital conversion (ADC) branches and each branch is connected to V_R antenna elements. Fig. 1 shows the system block diagram. Suppose there are N used subcarriers with indexes $k_1, \cdots, k_N$ where $k_i = -k_{N-i}$ and k_i for $i \leq N/2$ are negative. Define the frequency-domain signal vector at the TX DAC branch u_1 as $\mathbf{C}_{u_1} \triangleq [C_{u_1}[k_1], \cdots, C_{u_1}[k_N]]^T$ and that at the RX ADC branch u_2 as $\mathbf{Y}_{u_2} \triangleq [Y_{u_2}[k_1], \cdots, Y_{u_2}[k_N]]^T$. Then, we can express $\mathbf{Y}_{u_2}$ as

$$\mathbf{Y}_{u_2} = \sum_{u_1=1}^{U_T} \mathbf{A}_{u_2u_1}\mathbf{C}_{u_1} + \mathbf{B}_{u_2u_1}\mathbf{C}_{u_1}^* + \mathbf{W}_{u_2} \tag{1}$$

where $\mathbf{A}_{u_2u_1}$ and $\mathbf{B}_{u_2u_1}$ are components of the equivalent channel in the presence of RF distortions, and $\mathbf{W}_{u_2}$ is the noise vector. The significant elements of $\mathbf{A}_{u_2u_1}$ (due to channel, PN and CFO effects) would be around the main diagonal, thus taking a banded diagonal form while those of $\mathbf{B}_{u_2u_1}$ (due to IQI) would be around the anti-diagonal.

Define $\mathbf{C}_{R,u_1} \triangleq \Re\{\mathbf{C}_{u_1}\}$, $\mathbf{C}_{I,u_1} \triangleq \Im\{\mathbf{C}_{u_1}\}$, $\mathbf{Y}_{R,u_2} \triangleq \Re\{\mathbf{Y}_{u_2}\}$, $\mathbf{Y}_{I,u_2} \triangleq \Im\{\mathbf{Y}_{u_2}\}$, $\tilde{\mathbf{Y}}_{u_2} \triangleq [\mathbf{Y}_{R,u_2}^T, \mathbf{Y}_{I,u_2}^T]^T$, $\tilde{\mathbf{C}}_{u_1} \triangleq \left[\mathbf{C}_{R,u_1}^T, \mathbf{C}_{I,u_1}^T\right]^T$, $\boldsymbol{\eta}_{u_2} \triangleq \left[\Re\{\mathbf{W}_{u_2}\}^T, \Im\{\mathbf{W}_{u_2}\}^T\right]^T$, and

$$\mathbf{U}_{u_2u_1} \triangleq \mathbf{A}_{u_2u_1} + \mathbf{B}_{u_2u_1} \tag{2}$$

$$\mathbf{V}_{u_2u_1} \triangleq j(\mathbf{A}_{u_2u_1} - \mathbf{B}_{u_2u_1}). \tag{3}$$

Then we can express (1) in the real-valued form as

$$\tilde{\mathbf{Y}}_{u_2} = \sum_{u_1=1}^{U_T} \mathbf{Q}_{u_2u_1}\tilde{\mathbf{C}}_{u_1} + \boldsymbol{\eta}_{u_2} \tag{4}$$

where $\mathbf{Q}_{u_2u_1}$ is given by

$$\mathbf{Q}_{u_2u_1} \triangleq \begin{bmatrix} \Re\{\mathbf{U}_{u_2u_1}\} & \Re\{\mathbf{V}_{u_2u_1}\} \\ \Im\{\mathbf{U}_{u_2u_1}\} & \Im\{\mathbf{V}_{u_2u_1}\} \end{bmatrix}. \tag{5}$$

In (4), the effective channel between DAC branch u_1 and ADC branch u_2 is given by $\mathbf{Q}_{u_2u_1}$ which is a $2N \times 2N$ matrix. Note that $\mathbf{Q}_{u_2u_1}$ has significant elements only in the banded diagonal and anti-diagonal elements due to the properties of $\mathbf{A}_{u_2u_1}$ and $\mathbf{B}_{u_2u_1}$. Finally, by collecting the signal vectors from all ADC branches, the signal model can be expressed as

$$\tilde{\mathbf{Y}} = \mathbf{Q}\tilde{\mathbf{C}} + \boldsymbol{\eta} \tag{6}$$

where $\tilde{\mathbf{Y}} \triangleq \left[\tilde{\mathbf{Y}}_1^T \cdots \tilde{\mathbf{Y}}_{U_R}^T\right]^T$, $\tilde{\mathbf{C}} \triangleq \left[\tilde{\mathbf{C}}_1^T \cdots \tilde{\mathbf{C}}_{U_T}^T\right]^T$, $\boldsymbol{\eta} \triangleq \left[\boldsymbol{\eta}_1^T \cdots \boldsymbol{\eta}_{U_T}^T\right]^T$ and the (m,k) sub-matrix of $\mathbf{Q}$ is $\mathbf{Q}_{mk}$. $\mathbf{Q}$ is the equivalent channel matrix accounting for the channel, RF distortions, and analog beamforming. We insert OFDM symbol index n as $\mathbf{Y}_n$, $\mathbf{Q}_n$, $\mathbf{Q}_{ij,n}$, $\mathbf{A}_{u_2u_1,n}$, and $\mathbf{B}_{u_2u_1,n}$.

For channel and RF distortion compensation, we first obtain the estimate of $\mathbf{Q}_n$, denoted $\hat{\mathbf{Q}}_n$, by using two groups of pilots (described later). Then, we apply linear compensation as

$$\hat{\mathbf{C}}_n = \left(\hat{\mathbf{Q}}_n\right)^{\dagger}\mathbf{Y}_n \tag{7}$$

where $(.)^{\dagger}$ is the pseudoinverse operator.

III. Initial Design of Waveform Setting

As SC-FDE can be viewed as pre-coded OFDM, we will design the waveform parameters for OFDM. In particular, subcarrier spacing, DFT size, cyclic prefix (CP) interval, and pilot signals should be designed by taking into account RF distortions, channel environment, and overhead. We will select in this section a few candidate settings of the waveform for further detailed performance evaluation based on the following performance indicators:

Normalized PN bandwidth, PN power, and normalized CFO: The PN bandwidth normalized by the sub-carrier spacing (e.g., 90% power bandwidth $W_{\mathrm{pn},90}$) is an indicative of the inter-subcarrier interference (ICI) level due to PN, and is desired to be much smaller than 1. Similarly, the CFO normalized by the sub-carrier spacing reflects the level of CFO-induced ICI. Larger values of PN bandwidth, PN power, and normalized CFO favor a larger sub-carrier spacing.

Oversampling factor: For easy DAC and filter implementation, the sampling frequency at the output of IDFT of the OFDM system is desired to be reasonably larger than the nominal bandwidth of the signal. But this implies the same higher sampling frequency at the receiver ADC, and hence higher complexity.

CP overhead: The CP interval is typically set to be larger than the maximum time delay of the channel paths with non-negligible energy plus TX and RX filter spans and potential timing synchronization errors. To limit the overhead, the CP overhead ratio (i.e. the CP interval normalized by the OFDM symbol interval including CP) should be reasonably small which favors a smaller sub-carrier spacing.

Mobile speed: Mobile environments cause time-varying channels which could set a minimum limit on the sub-carrier spacing to maintain orthogonality among the sub-carriers.

Based on the above performance indicators and the system and channel specifications (250 MHz bandwidth and maximum channel delay spread of 80 ns), we selected four waveform parameter settings as shown Table I for performance evaluation. For a larger bandwidth, we can simply increase the DFT size and the number of used subcarriers while keeping the same subcarrier spacing, (e.g., for 2 GHz bandwidth, DFT size is 8 times that in the table). We use spectral square-root raised cosine (SRRC) filters for TX pulse shaping and RX filtering. Excluding the performance and capability of the ICI compensation scheme, we can assert that among the 4 systems, System 1 is the best in terms of CP overhead but the worst in view of ICI. System 4 is the best against ICI but the worst in terms of CP overhead. With ICI compensation scheme, their performances need to be investigated to find the best tradeoff, and we will describe the results in a later section.

IV. Pilots and Estimators for Compensation

We adopt our pilots and estimators from [23]. For completeness we briefly describe them. For more details, see [23].

A. Pilot Designs for Channel and Distortions Compensation

We consider pilot-aided estimation of significant elements of $\boldsymbol{Q}_n$.The pilot sequence transmitted is a low peak-to-average power ratio (PAPR) sequence, thus, we only define the sub carrier indexes. Suppose the indices of the used subcarriers are given by $-N_L, -N_L+1, \cdots, -l_1, l_1, \cdots, N_R$, and l_1 is the index of the used subcarrier most adjacent to the DC subcarrier. Typically, the DC subcarrier is not used and in this case $l_1 = 1$. Let $J^{\mathrm{L}}_{\mathrm{NZP},n}$ and $J^{\mathrm{R}}_{\mathrm{NZP},n}$ represent the subcarrier index set of the non-zero pilot tones at the left and right side of the DC tone in OFDM symbol n, respectively. Our pilots will use both non-zero and null pilot tones to facilitate easy estimation of the required equivalent channel matrix coefficients.

Type I: Pilot for main diagonal elements of $\boldsymbol{Q}_{ij,n}$: We choose pilot tone spacing D (in units of tones) as $D = \kappa + 1$ where κ represents the width of significant ICI spread to each side. We set $\kappa = 1$. Using MATLAB convention, we write $J^{\mathrm{R}}_{\mathrm{NZP},n} = l_1 : D : N_R$ and $J^{\mathrm{L}}_{\mathrm{NZP},n} = -(l_1+1) : -D : -N_L$. The final pilot design is given by $J_{\mathrm{NZP},n} = \{J^{\mathrm{L}}_{\mathrm{NZP},n}, J^{\mathrm{R}}_{\mathrm{NZP},n}\}$. The mirror index set of $J_{\mathrm{NZP},n}$ is denoted by $J_{\mathrm{NZPM},n} = -J_{\mathrm{NZP},n}$ and this pilot satisfies $J_{\mathrm{NZPM},n} \cap J_{\mathrm{NZP},n} = \emptyset$.

For K digital channels (the number of parallel spatial channels in digital beam forming), in general we need K preamble symbols where the preamble symbol n is transmitted on the digital channel n only.

Type II: Pilot for banded main diagonal elements and banded anti-diagonal elements of $\{\boldsymbol{Q}_{ij,n}\}$: This design uses $2V$ non-zero pilot tones in each pilot-data multiplexed symbol where the right side and the left side of the DC tone each has V non-zero pilot tones defined, respectively, by $\mathbf{p}^R = \mathbf{p}^L = [\mathbf{0}_{1\times\kappa}, \mathbf{1}_{1\times V} \otimes \mathbf{p}, \mathbf{0}_{1\times\kappa}]$ where $\otimes$ denotes the Kronecker product and $\mathbf{p}$ represents either basic pilot pattern template 1 defined by $[\mathbf{0}_{1\times\kappa}, 1, \mathbf{0}_{1\times\kappa}, 0]$ or template 2 defined by $[0, \mathbf{0}_{1\times\kappa}, 1, \mathbf{0}_{1\times\kappa}]$ where 1 represents a non-zero pilot while 0 denotes a null pilot. The non-zero pilot index set due to $\mathbf{p}^R$ is given by $J^R_{\mathrm{NZP},n}$ and that due to $\mathbf{p}^L$ is given by $J^L_{\mathrm{NZP},n}$. They are related such that $-J^L_{\mathrm{NZP},n} = J^R_{\mathrm{NZP},n} + \kappa + 1$ or $-J^L_{\mathrm{NZP},n} = J^R_{\mathrm{NZP},n} - \kappa - 1$ for the basic pilot template 1 or the template 2, respectively. We set $V = 3$.

We denote the pilot indexes of all pilots including non-zeros and zeros pilots in nth OFDM symbol in the left (right) side of DC tone by $J^{\mathrm{L}}_{\mathrm{P},n}$ ($J^{\mathrm{R}}_{\mathrm{P},n}$). We place $J^{\mathrm{L}}_{\mathrm{P},n}$ and $J^{\mathrm{R}}_{\mathrm{P},n}$ somewhere in the middle at each side of the DC tone.

For K digital channels, we use the truncated version of the above design, namely $\mathbf{1}_{1\times V} \otimes \mathbf{p}$, for each digital channel, cascade them in an FDM manner without any null tone or 1 null tone between them, and then add κ null tones at each edge of the cascaded pilots. The index set of the non-zero pilot tones for digital channel k will be denoted by $J^{(k)}_{\mathrm{NZP},n}$.

B. Estimation of Equivalent Channel Matrix

Estimation of main diagonal elements during preamble: We estimate the main diagonal of $\mathbf{U}_{u_2u_1}$, or equivalently main diagonal of $\mathbf{A}_{u_2u_1}$, at the pilot tone locations based on the preamble pilot symbols as

$$\hat{A}_{u_2u_1,n=u_1}[i,i] = \frac{Y_{u_2,n}[k_i]}{p_1[k_i]},\ k_i \in J^{(u_1)}_{\mathrm{NZP},u_1} \tag{8}$$

where $p_1[k_i]$ represents the type I pilot transmitted on subcarrier k_i. Then, $\{\hat{A}_{u_2u_1,n=u_1}[i,i]\}$ for $k_i \notin J^{(u_1)}_{\mathrm{NZP},u_1}$ are obtained by interpolation.

Estimation of common phase error (CPE) induced phase change: Based on the type II pilots at OFDM symbol $n > U_T$, we estimate the CPE induced phase change by

$$a_{u_2u_1,n} = \frac{\sum_{k_i \in J^{(u_1)}_{\mathrm{NZP},n}} \frac{Y_{u_2,n}[k_i]}{p_2[k_i]\ \hat{A}_{u_2u_1,u_1}[i,i]}}{|J^{(u_1)}_{\mathrm{NZP},u_1}|},\quad n > U_T \tag{9}$$

where $p_2[k_i]$ represents the type II pilot on subcarrier k_i.

Estimation of normalized ICI coefficients: Based on the type II pilots at OFDM symbol $n > U_T$, we estimate the normalized ICI coefficients for those elements at an ICI spread of d tones ($d \in \{\pm 1, \cdots, \pm\kappa\}$) as

$$b^d_{u_2u_1,n} = \frac{\sum_{k_i \in J^{(u_1)}_{\mathrm{NZP},n}} \frac{Y_{u_2,n}[k_i - d]}{Y_{u_2,n}[k_i]}}{|J^{(u_1)}_{\mathrm{NZP},n}|},\quad n > U_T. \tag{10}$$

Estimation of the mirror interference coefficient: Based on the type II pilots at OFDM symbol $n > U_T$, we estimate the mirror interference coefficient by

$$m_{u_2u_1,n} = \frac{\sum_{k_i \in J^{(u_1)}_{\mathrm{NZP},n}} \frac{Y_{u_2,n}[-k_i]}{Y^*_{u_2,n}[k_i]}}{|J^{(u_1)}_{\mathrm{NZP},n}|},\quad n > U_T \tag{11}$$

Obtaining main diagonal elements for pilot-data multiplexed symbols: The main diagonal elements at pilot-data

TABLE I
WAVEFORM PARAMETER SETTINGS

	System 1	System 2	System 3	System 4
Sub-carrier spacing (Δf)	360 kHz	720 kHz	1.44 MHz	2.88 MHz
DFT size	1024	512	256	128
DFT sampling frequency (f_s)	368.64 MHz	368.64 MHz	368.64 MHz	368.64 MHz
Bandwidth	250 MHz	250 MHz	250 MHz	250 MHz
No. of CP samples (@ f_s)	55	55	55	55
OFDM symbol interval ($T_{\rm sym}$) (CP included)	2.927 μs	1.538 μs	0.844 μs	0.496 μs
CP overhead	5.10%	9.70 %	17.68 %	30.05 %
Normalized coherence bandwidth ($W_{\rm coh}/\Delta f$)	17.36	8.68	4.34	2.17
Normalized CFO (1 ppm)	1.0139	0.5069	0.2535	0.1267
Normalized PN bandwidth ($W_{\rm pn,90}/\Delta f$)	0.6209	0.3104	0.1552	0.0776
Normalized coherence time ($T_{\rm coh}/T_{\rm sym}$)	126.36	240.47	438.41	745.06
No. of used sub-carriers (approx.) (DC tone excluded)	694	347	173	86
No. of used sub-carriers (integer multiple of 12)	684	336	168	84
SRRC filter roll-off	0.329	0.338	0.325	0.329
SRRC filter span (@ f_s)	12 samples	12 samples	12 samples	12 samples

multiplexed symbols are obtained from those at preamble symbol and the corresponding CPE induced phase change as

$$\hat{A}_{u_2u_1,n}[i,i] = a_{u_2u_1,n}\hat{A}_{u_2u_1,u_1}[i,i], \quad n > U_T. \tag{12}$$

Obtaining the banded diagonal elements (excluding main diagonal): Based on the estimates of normalized ICI coefficients, the banded diagonal elements at ICI spread of d tones are estimated as

$$\hat{A}_{u_2u_1,n}[i-d,i] = b^d_{u_2u_1,n}\hat{A}_{u_2u_1,n}[i,i] \tag{13}$$

for $d \in \{\pm 1, \cdots, \pm\kappa\}$ and $n > U_T$.

Obtaining anti-diagonal elements of $\hat{B}_{u_2u_1,n}$: Based on the mirror interference coefficient estimate, the anti-diagonal elements are estimated as

$$\hat{B}_{u_2u_1,n}[i,N-i] = m_{u_2u_1,n}\hat{A}^*_{u_2u_1,n}[N-i,N-i], \quad n > U_T. \tag{14}$$

Obtaining $\hat{\mathbf{Q}}_{u_2u_1,n}$: After estimating $\hat{\mathbf{A}}_{u_2u_1,n}$ and $\hat{\mathbf{B}}_{u_2u_1,n}$, we obtain $\hat{\mathbf{Q}}_{u_2u_1,n}$ for $n > U_T$ from (2), (3) and (5).

V. PERFORMANCE EVALUATION

Due to nonlinear distortions caused by several RF distortions, analytical performance assessment is intractable for the considered system. Thus, we rely on simulation based performance evaluation. We compare OFDM and SC-FDE (DFT-spread OFDM) in terms of BER performance, PAPR and power spectral density (PSD). [1] We consider both downlink (DL) and uplink (UL) OFDM with 64 antennas at BS and 4 antennas at UE at a carrier frequency of 73 GHz. The channel model is based on the 3GPP LTE channel model with two clusters where each cluster has 20 sub-paths, the second clusters delay is about 80 ns and its power is -9 dB with reference to the first cluster. Analog beamforming applies a phase shift beamformer (delay-and-sum beamforming [24]) in the direction of the average arrival angle of the 20 sub-paths of the first cluster where we assume such average arrival angle is known (can be estimated in an earlier phase). We consider a single and two digital channels with 16-QAM.

The systems settings are given in Table I (We also investigated with 2 GHz bandwidth and the results are similar and omitted here). Signals are generated in time domain with 4 times oversampling as in Fig. 1, while pilot designs, estimation and compensation are based on frequency domain model in Section II. The PN power spectral densities at transmit and receive sides are independently modeled as $\mathrm{PSD}(f) = \mathrm{PSD}(0)[1+(\frac{f}{f_z})^2]/[1+(\frac{f}{f_p})^2]$ where pole and zero frequencies f_p and f_z can be computed from PSD(0) = -60 dBc/Hz, PSD(f = 100 kHz) = -70 dBc/Hz and PSD(∞) = -130 dBc/Hz (based on measurement by Huawei). For the case with two data streams, the digital beamforming matrix is set as $\boldsymbol{I}_2$, and we use two incoherent phase noise groups. The CFOs at TX and RX sides are independent and uniformly distributed within the range of ± 1 ppm, the RX SFO is set at 1ppm and the RX STO is uniformly distributed within $[-T_{\rm rx}/2, T_{\rm rx}/2]$ where $T_{\rm rx}$ is the RX sampling period. IQIs are independent at TX and RX sides and they are uniformly distributed within the range defined by the maximum amplitude imbalance of 4 dB and the maximum phase imbalance of 5 degrees. The nonlinear power amplifier (PA) model is according to IEEE 802.11ad. The mobile speed is 10 km/h. The average SNR is set at 10 dB. The transmission frame has 7 OFDM symbols.

Fig. 2 presents the un-coded BER for DL systems with 9 dB PA output power backoff for $K = 1$ and 2 digital channels. The corresponding UL performances are similar and hence omitted. We observe the following. i) For both OFDM and SC-FDE waveforms with $K = 1$ digital channel, System 3 gives the best BER performance. This can be explained by the nature of the tradeoff between ICI levels and the accuracy level of the channel estimates (main diagonal elements of $\{\boldsymbol{Q}_{ij,n}\}$) as the sub-carrier spacing is changed. System 3 offers the best tradeoff among the 4 systems. ii) BER is degraded for $K = 2$ (increased data rate) if compared to $K = 1$ due to additional inter-stream interference. System 3 and System 4 give almost the same BER performance for $K = 2$ which could be ascribed to similar levels of inter-stream interference

[1] We also evaluated error vector magnitude (EVM) and found that the EVM results often experienced outliers and they were less informative than BER results, thus we omitted them.

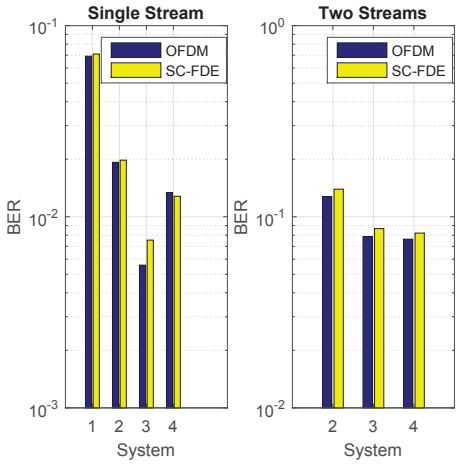

Fig. 2. Un-coded BER of systems with one and two data streams in DL

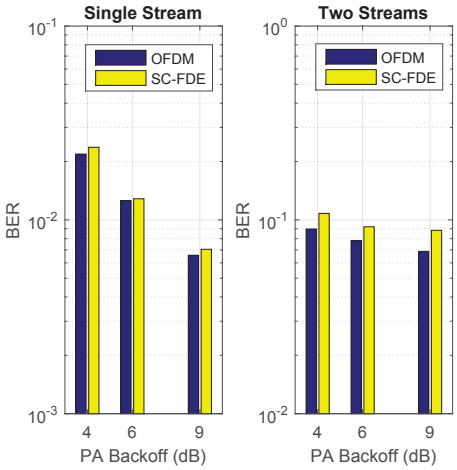

Fig. 3. Effects of PA backoff on un-coded BER of system 3 with one and two data streams in UL

which dominates the BER performance. iii) OFDM yields a slight BER advantage over SC-FDE[2].

Next in Fig. 3 we present the effects of PA backoff on uncoded BER for UL of system mode 3 with $K = 1$ and 2 digital channels. We have the following observations. i) The BER performance of OFDM is slightly better than that of SC-FDE (see footnote 2). ii) The BER performances degrade with a smaller PA output backoff for all cases. This is expected due to the increased non-linear distortion. iii) Decreasing the PA backoff from 9 dB to 6 dB almost doubles the BER for the one data stream case. Thus, an output backoff of 9 dB is preferred for one data stream with 16-QAM. iv) For the case with two data streams and 16-QAM, the increase in BER due to the relative decrease of PA backoff is mild. The reason could be that the inter-stream interference is more dominant than the incurred non-linear distortion. In this case, at least 6 dB PA output backoff is preferred.

In Fig. 4, we present the complementary cumulative distribution function (CCDF) of the PAPR of OFDM and SC-FDE waveforms at the input and the output of the PA with 4 dB and 9 dB backoff for system 3 in DL with RF distortions as well as at the input of the PA for the scenario without RF distortions. The UL performances are similar and hence omitted. We observe the following. i) RF distortions degrade PAPR characteristics of both waveforms and the PAPR performance advantage of SC-FDE over OFDM is slightly reduced in the presence of RF distortions. ii) The PAPR performance gap between OFDM and SC-FDE is not large and the reason can be ascribed to a large QAM size, SRRC TX filter and RF distortions. iii) The PAPR performance gap between the two waveforms becomes smaller after the PA which indicates that

[2]The frequency-selectivity of the considered mm-wave channel is mild, and IQI also introduces frequency diversity for OFDM. The SNR of interest for massive MIMO systems is medium or low. These facts make frequency-diversity exploitation advantage of SC-FDE over OFDM for uncoded system unfruitful. Also note that a large QAM size, DFT-spread oversampled OFDM processing, pulse-shape filtering, and IQI increase PAPR of SC-FDE to within 1 dB of OFDM. On the other hand, frequency-domain compensation/equalization yields better performance for OFDM. Overall, OFDM shows a slight BER advantage for the considered scenario.

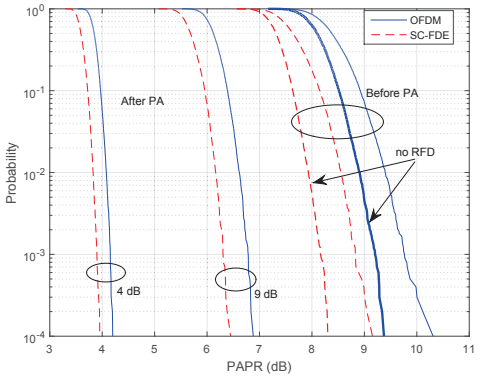

Fig. 4. The CCDF of the PAPR of OFDM and SC-FDE TX signals before and after the power amplifier for system 3.

the ADC requirement would not be much different for them.

Next, we present in Fig. 5 the average power spectral density (PSD) of OFDM and SC-FDE waveforms at the input and the output of the PA for DL of System 3 with RF distortions and 9 dB PA backoff and without RF distortions (same performance for UL). The PSD for the case with RF distortions and 4 dB PA backoff is shown in Fig. 6. In the figures, the x-axis index of 1024 corresponds to $4f_s = 4 \times 368.64$ MHz. The PSD plots show some spikes and drops within the signal bandwidth and they account for the boosted non-zero pilot tones and null pilot tones, respectively. We observe the following. i) For both waveforms, RF distortions increase the floor of PSD as well as the spectral broadening of the mainlobe. ii) In spite of some difference in PAPR characteristics, the PSDs are almost the same for both waveforms. This implies that the difference of PA-induced spectral broadening between the two waveforms is insignificant if compared to the level of spectral broadening caused by all RFD. iii) A smaller PA backoff causes larger PSD floor and mainlobe broadening for both waveforms.

VI. Conclusion

Millimeter-wave massive MIMO systems face strong RF distortions and complexity constraints due to the very high

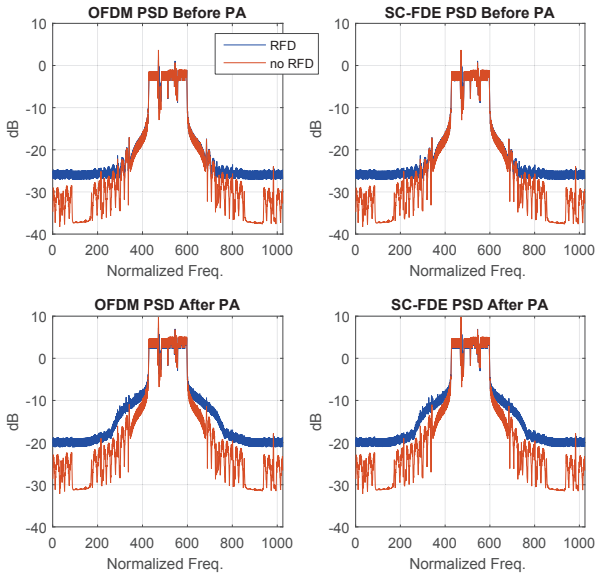

Fig. 5. The PSD of OFDM and SC-FDE TX signals before and after the amplifier with 9 dB backoff for system 3.

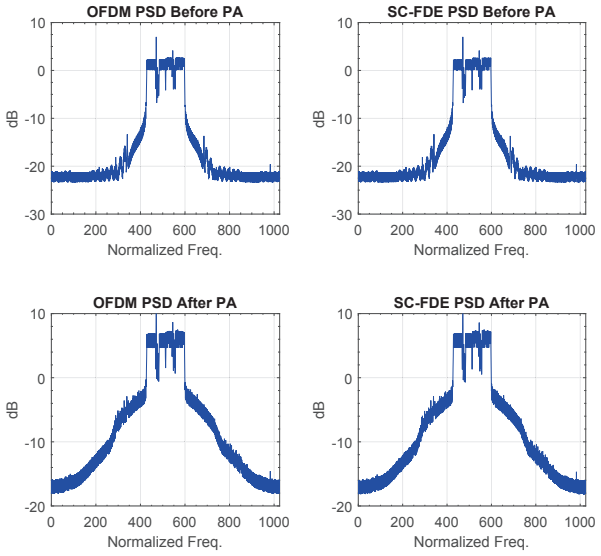

Fig. 6. The PSD of OFDM and SC-FDE TX signals before and after the amplifier with 4dB backoff for system 3.

sampling rate, which in turn influence the choice of the waveform and its parameter settings. In view of the complexity constraint, we selected OFDM and SC-FDE (DFT-spread OFDM) waveforms and studied their performance as well as their parameter settings for millimeter-wave massive MIMO systems with strong RF distortions at both TX and RX sides. Our results show that a proper choice of subcarrier spacing is important for such mmWave systems with strong PN, CFO, and IQI. Furthermore, TX RF distortions change the characteristics of PAPR and PSD for both waveforms, and slightly reduce the PAPR performance gap between OFDM and SC-FDE with 16-QAM. For both UL and DL, OFDM offers a slight uncoded BER advantage over SC-FDE, and the use of the same waveform for both UL and DL also reduces the complexity.

Acknowledgment: This work is partially supported by Huawei Technologies Co., Ltd., China.

REFERENCES

[1] S. Rangan, et al., "Millimeter-wave cellular wireless networks: Potentials and challenges," *Proc. IEEE*, vol. 102, no. 3, pp. 366–385, Mar. 2014.

[2] P. Banelli, et al., "Modulation formats and waveforms for 5G networks: Who will be the heir of OFDM?: An overview of alternative modulation schemes for improved spectral efficiency," *IEEE Signal Process. Mag.*, vol. 31, no. 6, pp. 80–93, Nov. 2014.

[3] N. Michailow, et al., "Generalized frequency division multiplexing for 5th generation cellular networks," *IEEE Trans. Commun.*, vol. 62, no. 9, pp. 3045–3061, Sept. 2014.

[4] B. Farhang-Boroujeny, "OFDM versus filter bank multicarrier," *IEEE Signal Process. Mag.*, vol. 28, no. 3, pp. 92–112, May 2011.

[5] G. Wunder, et al., "5GNOW: Non-orthogonal, asynchronous waveforms for future mobile applications," *IEEE Signal Process. Mag.*, vol. 52, no. 2, pp. 97–105, Feb. 2014.

[6] A. Ghosh, et al., "Millimeter-wave enhanced local area systems: A high-data-rate approach for future wireless networks," *IEEE J. Sel. Areas Commun.*, vol. 32, no. 6, pp. 1152–1163, June 2014.

[7] H. G. Myung, et al., "Peak-to-average power ratio of single carrier FDMA signals with pulse shaping," in *IEEE PIMRC*. Sept. 2006.

[8] G. Berardinelli, et al., "OFDMA vs. SC-FDMA: Performance comparison in local area IMT-A scenarios," *IEEE Wireless Commun.*, vol. 15, no. 5, pp. 64–72, Oct. 2008.

[9] T. Shi, et al., "Capacity of single carrier systems with frequency-domain equalization," in *Proc. IEEE Circuits and Systems Symp. Emerging Technologies: Frontiers of Mobile and Wireless Commun.*, vol. 2. May 2004, pp. 429–432.

[10] Y. Carmon, et al., "Comparison of the achievable rates in OFDM and single carrier modulation with iid inputs," *IEEE Trans. Inform. Theory*, vol. 61, no. 4, pp. 1795–1818, Apr. 2015.

[11] Z. Wang, et al., "OFDM or single-carrier block transmissions?" *IEEE Trans. Commun.*, vol. 52, no. 3, pp. 380–394, Mar. 2004.

[12] E. Yaacoub, et al., "A comparison of uplink scheduling in OFDMA and SCFDMA," in *IEEE Intl. Conf. Telecommun.*. Apr. 2010, pp. 466–470.

[13] V. Dalakas, et al., "A comparative study between SC-FDMA and OFDMA schemes for satellite uplinks," *IEEE Trans. Broadcast.*, vol. 58, no. 3, pp. 370–378, Sept. 2012.

[14] C. Ibars, et al., "A comparison of waveform candidates for 5G millimeter wave systems," in *Asilomar Conf.*, Nov. 2015, pp. 1747–1751.

[15] H. Huang, et al., "Phase noise and frequency offset compensation in high frequency MIMO-OFDM system," in *IEEE ICC*, June 2015, pp. 1280–1285.

[16] T. A. Thomas, et al., "Blind phase noise mitigation for a 72 GHz millimeter wave system," in *IEEE ICC*, June 2015, pp. 1352–1357.

[17] B. K. Ng, "The performance of SC-FDMA systems with rotated constellation in the presence of phase noise and channel estimation error," in *Intl. Conf. Wireless Commun. Signal Process.* , Oct. 2015.

[18] L. Fan, et al., "Joint IQ imbalance and PA nonlinearity pre-distortion for highly integrated millimeter-wave transmitters," *IEEE Globecom Workshops*, Dec. 2014, pp. 399–404.

[19] M. Wu, et al., "Hardware impairments in millimeter wave communications using OFDM and SC-FDE," *WSA 2016*, Mar. 9-11, 2016.

[20] A. G. Armada and M. Calvo, "Phase noise and sub-carrier spacing effects on the performance of an OFDM communication system," *IEEE Commun. Lett.*, vol. 2, no. 1, pp. 11–13, Jan. 1998.

[21] F. Schaich and T. Wild, "Subcarrier spacing - a neglected degree of freedom?" in *IEEE SPAWC*, June 2015, pp. 56–60.

[22] H. Wang, et al., "Perspectives on new waveform design for 5G small cell," in *General Assembly and Scientific Symp.*, Aug. 2014, pp. 1–4.

[23] A. Khansefid, et al., "Pilot designs and compensation scheme for severe RF distortions in millimeter-wave massive MIMO systems," *IEEE Globecom MCHFB Workshop 2016*.

[24] H. Van Trees, "Optimum Array Processing", New York: Wiley-Interscience, 2002.